

RESEARCH

Open Access



PRDX2 induces tumor immune evasion by modulating the HDAC3-Galectin-9 axis in lung adenocarcinoma cells

Yunjia Dong^{1,2}, Anqi Cheng^{1,3†}, Jiawei Zhou^{1,2}, Jianqiang Guo^{1,2}, Yafeng Liu^{1,3}, Xuan Li^{1,2}, Maoqian Chen^{1,2}, Dong Hu^{5,6*} and Jing Wu^{4*}

Abstract

Background PRDX2 is significantly expressed in various cancers and is associated with the proliferation of tumor cells. Nonetheless, the precise mechanism of PRDX2 in tumor immunity remains incompletely understood. This study aims to investigate the impact of PRDX2, which is highly expressed in lung adenocarcinoma, on T cells in the tumor immune microenvironment, and its immune action target to promote the immune escape of lung cancer cells, to provide a theoretical basis for lung adenocarcinoma treatment with PRDX2 as the target.

Methods Mouse animal models to verify the effect of Conoidin A treatment on tumor growth and T cell infiltration. Flow cytometry and Western blot verified tumor cell apoptosis in the in vitro co-culture system as well as granzyme B and perforin expression in T cells. RNA-Seq was used to obtain the downstream immune molecule. si-RNA knockdown of Galectin-9 was co-cultured with T cells in vitro. Immunofluorescence and Western blot verified that PRDX2 regulates Galectin-9 expression through HDAC3.

Results PRDX2 expression was negatively correlated with CD8⁺ T cell expression in LUAD patients. Inhibition of PRDX2 significantly enhanced T-cell killing of LUAD cells and reduced tumor load in both in vitro and in vivo models. Mechanistically, Conoidin A or shRNA_PRDX2 decreased Galectin-9 expression by down-regulating the phosphorylation of HDAC3, consequently enhancing the infiltration and function of CD8⁺ T cells.

Conclusions This study reveals the role of the PRDX2/HDAC3/Galectin-9 axis in LUAD immune escape and indicates Galectin-9 as a promising target for immunotherapy.

Keywords PRDX2, Lung adenocarcinoma, HDAC3, Galectin-9, Immune checkpoint

†Anqi Cheng: Co-first author.

*Correspondence:

Dong Hu

dhu@aust.edu.cn

Jing Wu

aust_jingwu@aust.edu.cn

¹School of Medicine, Anhui University of Science and Technology, Huainan, Anhui 232000, China

²Anhui Occupational Health and Safety Engineering Laboratory, Huainan, Anhui 232000, China

³Key Laboratory of Industrial Dust Deep Reduction and Occupational Health and Safety of Anhui Higher Education Institutes, Huainan, Anhui 232000, China

⁴Joint Research Center for Occupational Medicine and Health of IHM, School of Medicine, Anhui University of Science and Technology, Huainan, Anhui 232000, China

⁵The First Affiliated Hospital of Anhui University of Science and Technology (Huainan First People's Hospital, School of Medicine), Huainan, Anhui 232000, China

⁶Department of Laboratory Medicine, The First Affiliated Hospital of USTC, Division of Life Sciences and Medicine, University of Science and Technology of China, Hefei, Anhui 232001, China



Introduction

Lung cancer remains the most common malignancy and the leading cause of cancer-related deaths worldwide [1]. Non-small cell lung cancer (NSCLC) includes adenocarcinoma and squamous cell carcinoma, of which the most common histological subtype is lung adenocarcinoma (LUAD) [2, 3]. LUAD progresses rapidly and is often associated with distal metastases, leading to poor treatment outcomes and low survival rates. In recent years, immune checkpoint blockade therapy (ICB) has shown significant benefits in the treatment of advanced NSCLC [4], especially immune checkpoint inhibitors targeting programmed cell death protein 1 (PD-1)/programmed death receptor-1 (PD-L1) or cytotoxic T-lymphocyte-associated protein 4 (CTLA-4) are used for the treatment of multiple tumor types [5, 6], but clinical data suggest that the remission rate for patients treated with CTLA-4 blockers is approximately 15% [4, 7–9], and those targeting PD-1/PD-L1 rarely exceed 40% with a positive response [10]. immunotherapeutic targets to develop the anti-tumor potential of T cells further to benefit more patients. In this study, we sought to discover novel immune checkpoint pathways and mechanisms that could be used in cancer immunotherapy.

The peroxiredoxin (PRDX) family exhibits peroxidase activity and is ubiquitously present in almost all organisms [11]. PRDX can be categorized into three subfamilies (typical 2-Cys, atypical 2-Cys, and 1-Cys) based on the number and location of reactive cysteine residues and the type of disulfide bonds generated during the catalytic process [12, 13]. PRDX2 acts as a typical 2-Cys antioxidant enzyme, offering cellular protection from oxidative stress by eliminating H_2O_2 and regulating reactive oxygen species (ROS) levels [14]. PRDX2 shows high expression in various tumors, such as gastric cancer [15], colorectal cancer [16], and lung cancer [17]. The heightened expression of PRDX2 is also associated with the survival and proliferation of cancer cells, and patients with high PRDX2 expression tend to have a poorer prognosis than those with low expression. However, the involvement of PRDX2 in tumor immunity remains uncertain.

Galectin-9 belongs to the galactose family of animal lectins and possesses a conserved carbohydrate recognition domain (CRD) for β -galactosides. Structurally, it consists of two CRDs linked by a specific sequence [18]. Galectin-9, originally identified as a ligand for TIM-3, induces T cell death and its elevated expression has been associated with depleted T cell terminal differentiation subtypes [19, 20]. Galectin-9 promotes immunosuppression in the tumor microenvironment through interaction with cell surface receptors on immune cells. It is expressed in antigen-presenting cells (APCs) and can be induced by interferon (IFN) β and γ in tumor cells [21]. High expression of Galectin-9 is associated with various

cancers and low patient survival [22]. However, its role in immunotherapy and its potential as a therapeutic target requires further exploration.

This study found that PRDX2 is highly expressed in LUAD and impairs anti-tumor immunity in LUAD. Through in vivo animal studies, we found that inhibiting the anti-tumor effects of PRDX2 relies on the intact immune system. By conducting T cell-mediated tumor-killing assays, we have identified that PRDX2 can elevate Galectin-9 expression through HDAC3, thus inhibiting the tumor-killing function of T cells and facilitating immune evasion. Our findings shed light on the role of PRDX2 in immune escape in LUAD, thereby offering a potential approach for treating LUAD.

Materials and methods

Network databases

The TIMER database (<https://cistrome.shinyapps.io/timer/>) was used to analyze the differences in PRDX2 expression and the correlation between PRDX2 expression and the infiltration of six types of immune cells (B cells, $CD4^+$ T cells, $CD8^+$ T cells, neutrophils, macrophages, and dendritic cells) in pan-cancer. The TIMER2.0 database (<http://timer.cistrome.org>) were used to analyze the correlation between PRDX2 expression and $CD8^+$ T cell infiltration in pan-cancer. The KM-Plotter database (<http://kmplot.com>) was utilized to analyze PRDX2 expression levels in lung adenocarcinoma and lung squamous carcinoma and the prognosis of patients. RNAseq data of TCGA-LUAD were downloaded from the TCGA database (<https://portal.gdc.cancer.gov>) and collated to analyze PRDX2 expression disparities in LUAD paired and unpaired samples. The HPA database (<https://www.proteinatlas.org/>) investigated PRDX2 protein expression levels in lung adenocarcinoma and normal lung tissues.

Human tissue samples

Clinical lung adenocarcinoma samples were provided by the Cancer Hospital affiliated with Anhui University of Science and Technology, and all collected samples were used for the study after the patients signed an informed consent form. The study was approved by the Medical Ethics Committee of Anhui University of Science and Technology and was conducted following the principles of the Declaration of Helsinki (NO. HX-002).

Cell culture

The human embryonic kidney cell line HEK293T, human lung adenocarcinoma cell lines (A549, 95-D, H292, and H1975), and the mouse Lewis lung cancer cell line (LLC) were obtained from ATCC. A549, 95-D, H292, and H1975 cells were cultured in RPMI-1640 medium (Gibco) supplemented with 10% fetal bovine serum (FBS, Lonsera) and 1% penicillin/streptomycin (Beyotime) in

RPMI-1640 medium (Gibco). HEK293T cells and LLC cells were cultured in DMEM medium (Gibco) supplemented with 10% fetal bovine serum (FBS, Gibco) and 1% penicillin/streptomycin (Beyotime).

Plasmids and vectors

To generate stable transfected cell lines, short hairpin RNAs (shRNAs) targeting PRDX2 were synthesized by Sangon Biotech (Shanghai, China) and inserted into the shRNA expression vector pLVX-shRNA (Sangon Biotech, Shanghai, China). For transient transfection, siRNAs targeting PRDX2 and LGALS9 were obtained from GenePharma (Shanghai, China). The oligonucleotide sequences used are shown in Supplementary Table 1.

Cell transfections

293T cells were transfected with Lipofectamine 2000 Reagent (Invitrogen), PsPax2 (Fenghui Biotechnology, Hunan, China), PMD-2 g (Fenghui Biotechnology), and shRNA-PRDX2 plasmids according to the manufacturer's instructions, and the viral fluids were collected after 48 h.

For transfection of lentivirus-based constructs, 80% confluent H1975 and H292 cells were incubated for 24 h in a medium containing a concentrated viral solution and polyglutamine (Solarbio, H8761). Transfected cells were allowed to grow for a further 2 days and then selected with puromycin (1 µg/ml) (Sigma-Aldrich) for 1 week. Transfection efficiency was assessed by RT-qPCR and Western blot.

Cells with 60–80% confluence were transfected with Lipofectamine 2000 and siRNAs. Cells were incubated for 24–48 h and harvested for subsequent experiments.

RNA extraction and RT-qPCR

Total RNA was isolated using TRIzol (Invitrogen) and reverse transcribed using RevertAid First Strand cDNA Synthesis Kit (Thermo Scientific). The cDNAs were subjected to RT-qPCR using the 2X Universal SYBR Green Fast QPCR Mix System. Primers were designed and synthesized in collaboration with Sangon Biotech (Shanghai). Relative mRNA expression was calculated using the $2^{-\Delta\Delta C_t}$ method with GAPDH as a control. The sequences of the primers used are listed in Supplementary Table 2.

Western blot analysis

Total proteins were extracted by adding RIPA lysate (Beyotime, P0013C) containing protease inhibitors to the cells, and protein concentrations were determined using a BCA kit (Beyotime, P0012). Proteins were separated using SDS-PAGE and transferred to a polyvinylidene difluoride membrane (PVDF, Millipore, ISEQ00010). After transferring the membranes, they were blocked with a blocking solution containing 5% skimmed milk powder for 1 h at room temperature, incubated with

primary antibodies at 4 °C overnight, and then incubated with secondary antibodies conjugated with horseradish peroxidase (HRP) for 1 h at room temperature. Membranes were developed using an Amersham ImageQuant™ 800 Imaging System (Cytiva) and ECL luminescent solution (Millipore, WBKLS100). The primary and secondary antibodies used are listed in Supplementary Table 3.

Immunofluorescence and immunohistochemical

For multiplex immunofluorescence, paraffin sections were deparaffinized to water and blocked with 3% BSA after antigen repair in the EDTA antigen repair buffer (pH 8.0). The sections were then incubated overnight at 4 °C with the corresponding primary antibody in a humidified chamber, followed by incubation with the corresponding fluorescent secondary antibody for 1 h at room temperature. Each primary antibody was stained separately, and between each staining, the tissue sections were heated in a microwave oven in a repair cassette filled with EDTA antigen repair buffer (pH 8.0) to repair the antigen again. The nuclei were then restained by incubation with DAPI solution for 10 min at room temperature, protected from light. Finally, the sections were sealed with an anti-fluorescence quenching mounting medium. The images were detected and captured by inverted fluorescence microscopy (Leica 3000) and analyzed by Image J.

For immunohistochemistry, the paraffin sections were deparaffinized to water, the antigen was repaired with EDTA antigen repair solution, endogenous peroxidase was blocked with 3% hydrogen peroxide, and washed and blocked with 3% BSA. After adding the corresponding primary antibody, they were incubated at 4 °C overnight, followed by adding the corresponding secondary antibody (HRP labeled) and incubating at room temperature for 1 h. Subsequently, DAB was added to develop the color, hematoxylin re-staining of the nucleus was performed, and finally, the sections were dehydrated and sealed. The images were captured using an inverted fluorescence microscope (Leica 3000) and analyzed using Image J.

T cell-mediated tumor cell killing assay

To isolate PBMCs, 5 mL of venous blood was collected from healthy volunteers. Human blood collection was approved by the Medical Ethics Committee of Anhui University of Science and Technology, and written informed consent was obtained from all volunteers. PBMCs were obtained from peripheral blood using human peripheral blood lymphocyte isolate (TBD, LTS1077). To obtain activated T cells, PBMC were incubated in RPMI-1640 medium supplemented with 10% fetal bovine serum and 1% penicillin/streptomycin with ImmunoCult Human CD3/CD28/CD2 T cell activator (STEMCELL Technologies, 10970) and recombinant human IL-2 (PPL,

PK0119) were cultured together and activated for one week according to the manufacturer's protocol. NSCLC cells were inoculated into 6-well plates at the appropriate concentration. After 24 h, activated PBMCs were co-cultured with adherent NSCLC cells at a 3:1 ratio for 48 h. After 48 h of incubation, cell debris was removed, and T cells and NSCLC cells were collected separately for subsequent experiments.

Flow cytometry

To detect apoptosis, NSCLC tumor cells obtained by sorting with Dynabeads™ CD3 magnetic beads (Invitrogen, 1151D) after co-culture with T-cells, we utilized the Annexin V-FITC/PI Apoptosis Detection Kit (keyGEN BioTECH, KGA108) for double staining. Subsequently, the stained cells were examined using the FACSCanto II flow cytometer (BD, USA).

For the determination of Granzyme B expression in T cells, CD3 and CD8 antibodies were used to label cell surface expression of CD3 and CD8, and after fixation and permeabilization by Intracellular Fixation & Permeabilization Buffer Set (eBioscience, 88-8824-00), followed by staining for intracellular Granzyme B using the GZMB antibody. The stained cells were then analyzed by FACSCanto II flow cytometer, and the data were further analyzed using Flow Jo 10.0 software.

RNA sequencing

For Sh-PRDX2 H1975 lung adenocarcinoma cells and control, total RNA was extracted using TRIzol reagent (Invitrogen). After establishing sequencing libraries, we performed the 2 × 150 bp paired-end sequencing (PE150) on an Illumina Novaseq™ 6000 (LC-Bio Technology CO., Ltd., Hangzhou, China) following the vendor's recommended protocol.

In vivo study

All animals were housed in a 12-h light/12-h dark environment with controlled temperature cycles (22 ± 1 °C) and humidity (40 ± 5%). LLC cells were injected subcutaneously in BALB/c nude mice for the immunodeficient mouse model and in C57BL/6 mice for the immune-competent mouse model. When the tumor volume reached 100 mm³, saline-treated mice were used as the control group, and the experimental group was treated with Conoidin A (5 mg/kg or 10 mg/kg), once a day for 15 consecutive days. The tumor volume was measured with calipers every 3 days during the administration period and was calculated as follows: length × width² × 0.5. On the next day of the last administration, the mice were artificially executed by cervical dislocation, and the tumors were isolated and measured. All animal experiments were performed strictly with the NIH Guide for the Care and Use of Laboratory Animals, and the Medical Ethics

Committee of Anhui University of Science and Technology approved the animal experiments.

Statistical analysis

The data are presented as the mean ± SD. Data analysis was performed using GraphPad Prism 9. Unpaired or paired two-tailed Student's t-tests were conducted to compare the two groups. All experiments were repeated at least three times. Statistical significance was set at $P < 0.05$.

Results

PRDX2 is highly expressed in LUAD and inhibits CD8⁺ T cell infiltration in LUAD

To investigate the expression of PRDX2 in cancer, we first utilized the TIMER database to analyze the expression of PRDX2 in pan-cancer. The results showed that PRDX2 was differentially expressed in various cancers, and the expression level of PRDX2 was higher in LUAD and LUSC tissues than in normal tissues (Fig. 1A). Kaplan-Meier survival analysis indicated that high PRDX2 expression was associated with poorer prognosis in LUAD patients, while no significant difference was observed in LUSC patients (Fig. 1B-C). These results suggest that PRDX2 expression is closely related to the prognosis of LUAD patients. Further analysis of TCGA database data for LUAD paired and unpaired samples demonstrated significantly elevated PRDX2 expression in tumor tissues compared to normal lung tissues (Fig. 1D). We also observed notably higher expression in tumor tissues by using the HPA database to examine PRDX2 protein expression in LUAD and normal lung tissues (Fig. 1E). To explore the association of PRDX2 with immune infiltration, we utilized the TIMER database to assess the potential relationship between PRDX2 gene expression and immune cell infiltration in lung adenocarcinoma. Our findings revealed a negative correlation between PRDX2 expression and B cells, CD8⁺ T cells, CD4⁺ T cells, macrophages, neutrophils, and dendritic cells (Fig. 1F). Afterwards, the Timer2.0 database was used to analyze the correlation between PRDX2 expression in pan-cancer and CD8⁺ T-cell infiltration using various immunological algorithm, and the results showed that PRDX2 expression was negatively correlated with CD8⁺ T-cell infiltration in LUAD. (Supplementary Fig. 1A). Subsequent validation with clinical samples showed that PRDX2 was primarily localized in the cytoplasm, and its expression was inversely correlated with CD8⁺ T cell infiltration (Fig. 1G-H). Similarly, PRDX2 expression negatively correlated with CD3⁺ T cell infiltration, while no significant correlation with macrophages was observed (Supplementary Fig. 1B-E).

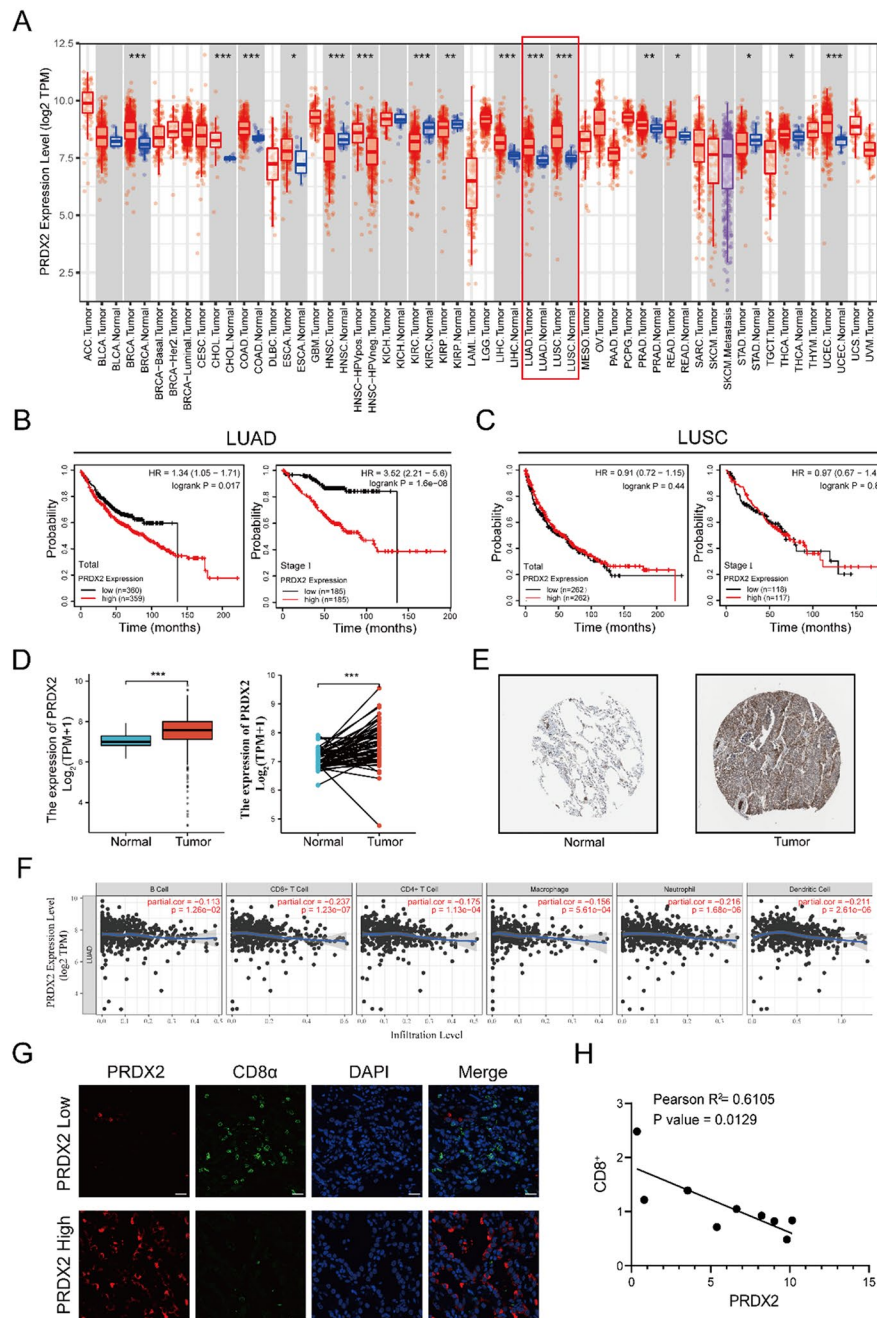


Fig. 1 PRDX2 is highly expressed in LUAD and negatively correlates with CD8⁺ T cell infiltration in LUAD patients. **(A)** PRDX2 expression in pan-cancer tumor tissues and normal tissues based on the TIMER database. **(B-C)** The correlation analysis of PRDX2 in LUAD **(B)** and LUSC **(C)** total and stage I patients' prognoses is based on the KM-Plotter database. **(D)** mRNA expression in LUAD and normal tissues based on the TCGA database. **(E)** HPA database analysis of PRDX2 protein level expression in LUAD and normal tissues. **(F)** Correlation analysis of PRDX2 expression with immune infiltration in LUAD based on the TIMER database. **(G)** Immunofluorescence staining of LUAD tissues for CD8⁺ T cells (CD8 α , green), PRDX2 localization (PRDX2, red), and nuclear staining (DAPI, blue). Scale bar = 20 μ m. **(H)** Analysis of the correlation between PRDX2 and CD8 expression. ns, not significant; $P > 0.05$, $*P < 0.05$, $**P < 0.01$, $***P < 0.001$

PRDX2 inhibitors reduce tumor load and enhance intratumor T cell infiltration in immune-competent mice

To investigate the impact of PRDX2 on lung adenocarcinoma tumor immunity, we established a lung cancer ectopic implantation model for in vivo studies in mice.

LLC cells were injected subcutaneously into immunodeficient mice (BALB/c nude mice) to form tumors, which were then treated by gavage administration of the PRDX2 inhibitor Conoidin A (5 mg/Kg or 10 mg/kg), with saline treatment serving as a control group (Fig. 2A).

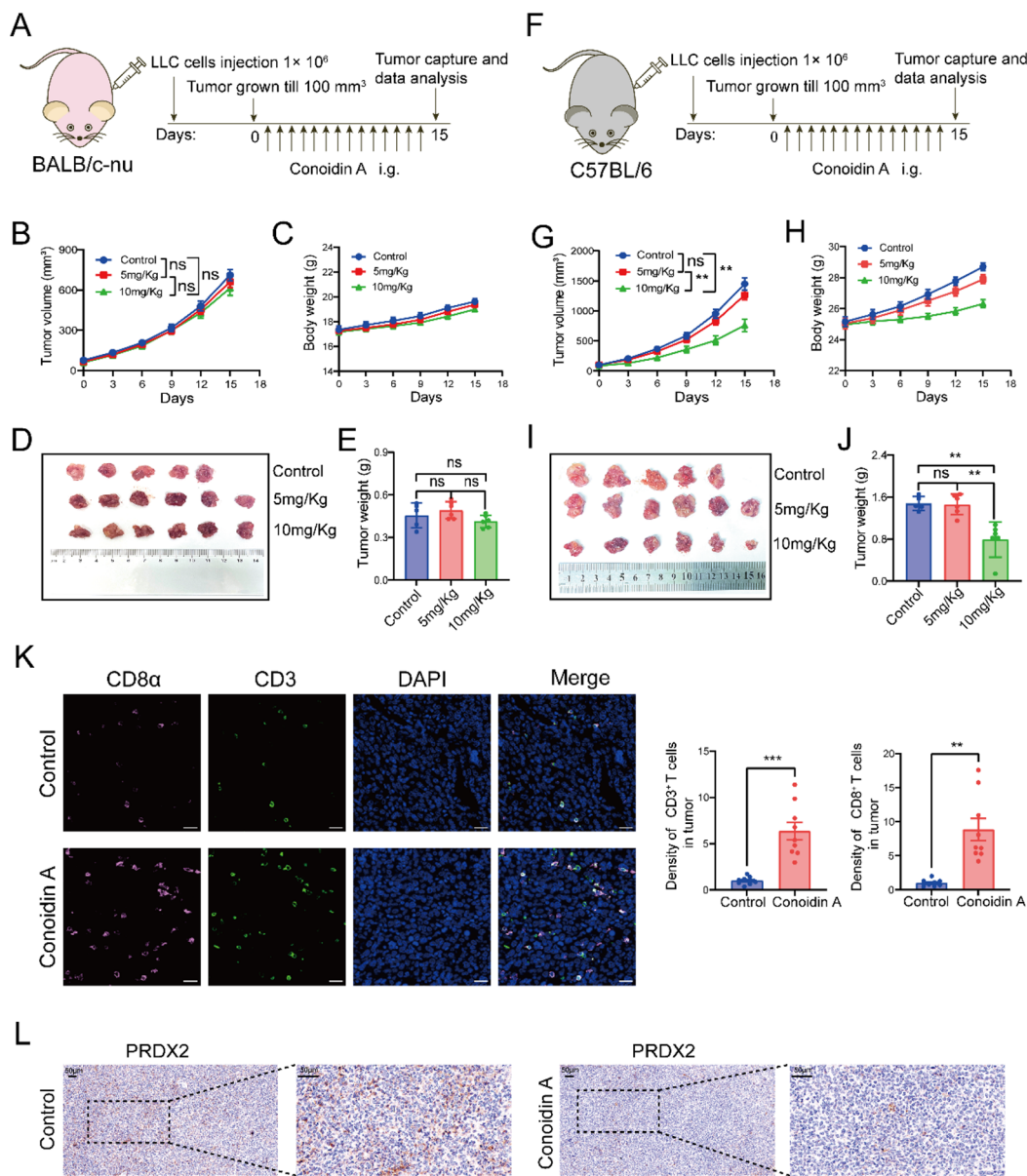


Fig. 2 Conoidin A diminishes tumor load and enhances CD8 $^+$ T cell infiltration in immunoreactive mice. **(A-E)** BALB/c nude mice were inoculated with 1×10^6 LLC cells and treated with 5 mg/Kg or 10 mg/Kg Conoidin A, while saline treatment served as the control group. **(A)** Schematic representation of the treatment regimen. **(B)** The plot depicts tumor volume measured every 3 days. **(C)** Mice body weight. **(D)** Pictures of tumors harvested after euthanasia of mice. **(E)** Tumour volume data after euthanasia. **(F-J)** C57BL/6 mice were inoculated with 1×10^6 LLC cells and treated with 5 mg/Kg or 10 mg/Kg Conoidin A, while saline treatment served as the control group. **(F)** Schematic representation of the treatment regimen. **(G)** Plot depicting tumor volume measured every 3 days. **(H)** Mice body weight. **(I)** Pictures of tumors harvested after euthanasia of mice. **(J)** Tumor volume data after euthanasia. **(K)** IF staining and quantification of the relative expression of CD3 $^+$ T cells and CD8 $^+$ T cells in tumor tissues of mice in the Control group and 10 mg/Kg Conoidin A treatment group. CD8 $^+$ T cells (CD8 α , pink), CD3 $^+$ T cells (CD3, green), and nuclear staining (DAPI, blue). Three mice per group were selected for IF staining and three fields of view per mouse were selected for analysis, with each dot representing one field of view. Scale bar = 20 μm . **(L)** IHC staining of PRDX2 in tumor tissues of mice in Control and 10 mg/Kg Conoidin A treatment groups. Scale bar = 50 μm . ns, not significant; $P > 0.05$, $*P < 0.05$, $**P < 0.01$, $***P < 0.001$

We observed no significant difference in tumor growth between the 5 mg/kg and 10 mg/kg Conoidin A treatment groups compared to the control group in BALB/c

nude mice (Fig. 2B-E). Additionally, to evaluate the role of the intact immune system in inhibiting PRDX2-mediated antitumor effects, we also injected LLC cells

subcutaneously into immunocompetent C57BL/6 mice (Fig. 2F). In C57BL/6 mice, no significant difference in tumor growth was observed in the 5 mg/Kg Conoidin A treatment group compared to the control group. In comparison, tumor growth was significantly inhibited in the 10 mg/Kg Conoidin A treatment group without any significant toxic effects (Fig. 2G-J).

Furthermore, immunofluorescence staining revealed a significant increase in CD3⁺CD8⁺ T-cell infiltration in tissues after treatment with 10 mg/kg Conoidin A (Fig. 2K). Similarly, immunohistochemical staining indicated that 10 mg/Kg Conoidin A significantly inhibited PRDX2 expression in immune-competent mice (Fig. 2L). This study demonstrated that the inhibition of PRDX2 impeded tumor progression in C57BL/6 immune-competent mice but did not slow tumor growth in BALB/c nude mice. These findings suggest that reducing tumor load induced by PRDX2 inhibition requires T lymphocyte engagement and that an immune system lacking mature T lymphocytes impairs the anti-tumor efficacy of PRDX2 deficiency.

Knockdown of PRDX2 sensitizes LUAD cells to T-cell-mediated cell death

To confirm the role of PRDX2 in LUAD anti-tumor immunity, we detected the expression level of PRDX2 in four lung adenocarcinoma cell lines (A549, 95-D, H292, H1975). The RT-qPCR results revealed significantly higher levels of PRDX2 protein expression in 95-D, H292, and H1975 cells (Fig. 3A). Similarly, Western blot results demonstrated elevated PRDX2 protein expression levels in H1975 cells, followed by H292 cells, with lower expression observed in A549 and 95-D cells (Fig. 3B). Subsequently, we constructed sh-RNA and si-RNA sequences targeting PRDX2 to knock down its expression in the LUAD cell lines. Both RT-qPCR and Western blot results confirmed that treatment with a plasmid targeting PRDX2 (sh-PRDX2) significantly reduced the expression level of PRDX2 in H1975 and H292 cells compared to cells in the sh-NC group. Among the sh-PRDX2 sequences, sh-PRDX2#2 showed the most effective knockdown of PRDX2 (Fig. 3C-D). Subsequently, among the three designed si-PRDX2 sequences, si-PRDX2#3 showed the most efficient knockdown in H1975 cells, whereas si-PRDX2#1 showed the most efficient knockdown in H292 cells, and on balance, we selected si-PRDX2#1, which had excellent knockdown efficiencies in both cell lines, for the subsequent experiments (Supplementary Fig. 2A-B). Consequently, we selected the best knockdown sequence for further experiments. We utilized MTS assays to assess the impact of PRDX2 knockdown on the growth and proliferation of the LUAD cell line. The results indicated that solely knocking down or not knocking down PRDX2 had no significant effect on

the proliferation of the LUAD cell line (Supplementary Fig. 2C-D).

In the following step, we carried out T cell-mediated tumor cell killing assays to illustrate the impact of PRDX2 knockdown on sensitizing LUAD cells to T cell-mediated cytotoxicity. Crystal violet staining and cell counting results indicated that the optimal ratio for the co-culture system was LUAD cells: T cells = 1:3 and the co-culture duration was 48 h (Supplementary Fig. 2E-H). Subsequent cell assays involved co-culturing H1975 and H292 cells with T cells at a 1:3 ratio for 48 h. Flow cytometry analysis for apoptosis detection revealed a significantly higher rate of apoptosis in the PRDX2 knockdown group than in the control group (Fig. 3E-F). Previous studies have shown that PARP serves as a cleavage substrate of caspase, a pivotal member of apoptosis, and represents the primary target caspase-3 *in vivo* [23]. The cleavage of PARP by caspase-3 deactivates PARP and suppresses its DNA repair capability. Therefore, cleaved PARP can be considered a marker of apoptosis [24]. Consequently, Western Blot was utilized to detect the expression of apoptosis-related proteins such as PARP, Cleaved-PARP, and cleaved-Caspase3. The results showed that apoptosis of LUAD cells with PRDX2 knockdown was not obvious. However, after co-culture with T cells, the expression of Cleaved-PARP and cleaved-Caspase3 proteins was increased in the cells of the PRDX2 knockdown group compared with the control group, and the expression of PARP protein was basically unchanged. This suggests that the increase in apoptosis in the PRDX2 knockdown group was evident in the co-culture system with, but not in the cell lines knocked down PRDX2 alone (Fig. 3G-H). Similarly, crystal violet staining results indicated that PRDX2 knockdown heightened the susceptibility of tumor cells to T-cell killing (Fig. 3I-J). These findings affirm that PRDX2 knockdown augmented the sensitivity of LUAD cells to T-cell killing.

Depletion of PRDX2 promotes CD8⁺ CTL-mediated tumor cell killing

We then investigated the effect of PRDX2 on the immunosuppressive activity of tumor cells on CD8⁺ T cells. The effect was assessed by examination of granzyme B (GZMB) levels and perforin expression in T cells. The flow cytometry analysis revealed elevated GZMB expression in CD3⁺CD8⁺ T cells after co-culture with PRDX2 knockdown lung adenocarcinoma cells (Fig. 4A-D). Furthermore, Western blot analysis was utilized to measure the protein expression of GZMB and perforin in T cells after *in vitro* co-culture. The results demonstrated a significant upregulation of GZMB protein and perforin in T cells co-cultured with the PRDX2 knockdown group (Fig. 4E-H). Similarly, immunofluorescence results indicated increased expression of GZMB and perforin in the

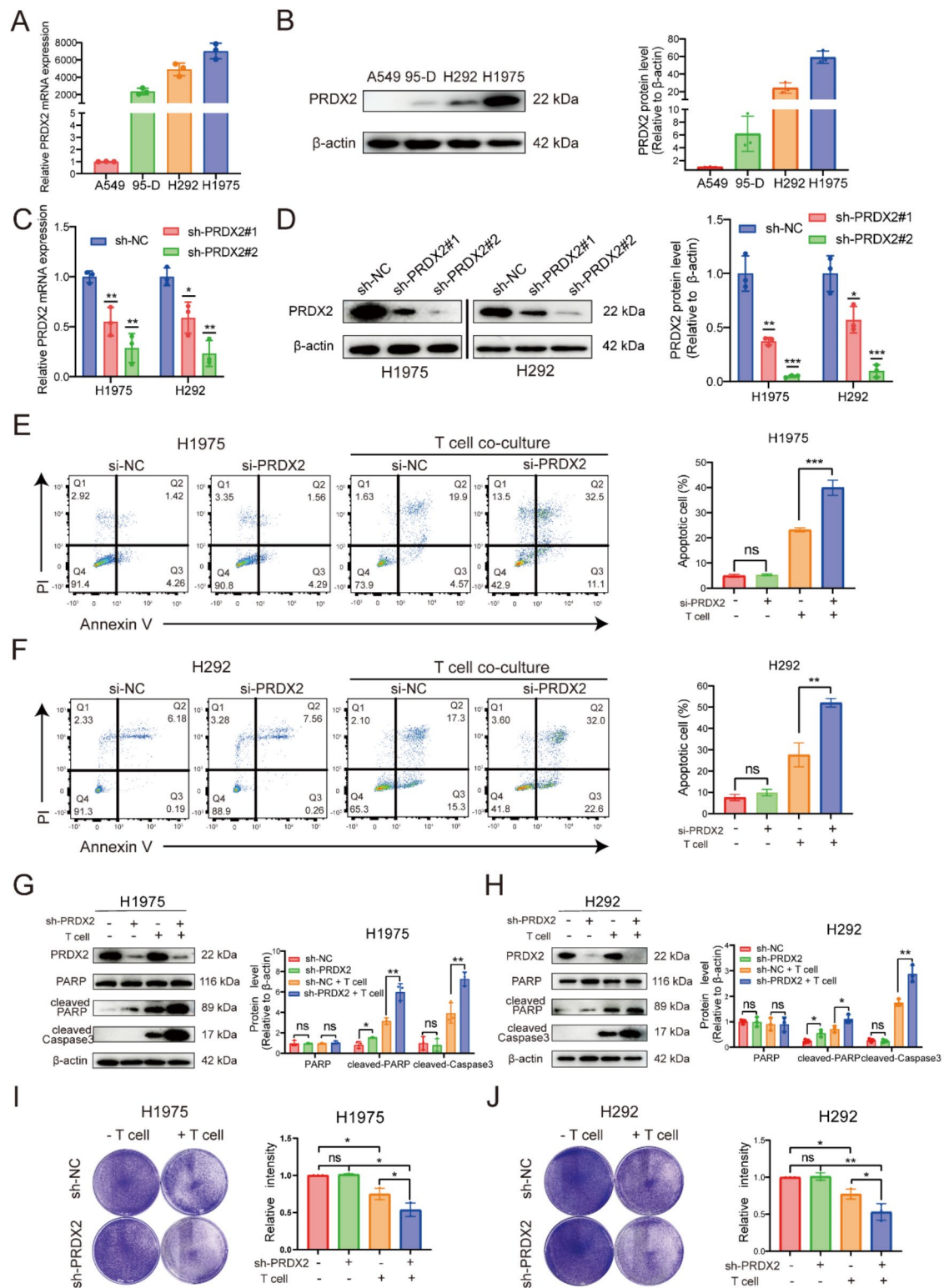


Fig. 3 (See legend on next page.)

(See figure on previous page.)

Fig. 3 Downregulation of PRDX2 enhances the susceptibility of LUAD cells to T cell-mediated apoptosis. **(A)** RT-qPCR detection of mRNA expression levels of PRDX2 in A549, 95-D, H292, and H1975 cell lines. **(B)** Protein expression levels of PRDX2 in A549, 95-D, H292, and H1975 cell lines (left) and their statistical quantitative analysis (right). **(C-D)** Evaluation of PRDX2 expression in H1975 and H292 cell lines transfected with sh-NC plasmid or sh-PRDX2 plasmid. **(C)** RT-qPCR analysis of PRDX2 mRNA expression levels in stably transfected H1975 and H292 cell lines. **(D)** Western blot analysis of PRDX2 protein levels in H1975 and H292 cell lines (left) and statistical analysis (right). **(E-F)** Representative images and statistical quantification of flow cytometry analysis of T cell-mediated apoptosis in LUAD cells as determined by Annexin V-FITC and propidium iodide (PI) double labeling. **(E)** Apoptosis visualization (left) and corresponding statistical analyses for PRDX2 knockdown and no knockdown in the H1975 cell line. **(F)** Apoptosis visualization for PRDX2 knockdown and no knockdown in the H292 cell line (left) and corresponding statistical analyses (right). **(G-H)** Detection of apoptotic protein expression in LUAD cells co-cultured with activated T cells for 48 h using Western blot. **(G)** Protein expression levels of PRDX2, PARP, cleaved-PARP, and cleaved-caspase3 (left) and corresponding statistical analyses (right) in the H1975 cell line with or without PRDX2 knockdown. **(H)** Protein expression levels of PRDX2, PARP, cleaved-PARP, and cleaved-caspase3 (left) and corresponding statistical analyses (right) in the H292 cell line with or without PRDX2 knockdown. **(I-J)** T cell-mediated LUAD cell killing assay. LUAD cells were co-cultured with activated T cells for 48 h, followed by crystal violet staining, and bar graphs indicate the normalized ratio of live cells per well. **(I)** Crystal violet staining showed the H1975 cell line co-cultured with T cells (left) and the corresponding normalized proportion of living cells (right). **(J)** Crystal violet staining showed the H292 cell line co-cultured with T cells (left) and the corresponding normalized proportion of living cells (right). ns, not significant; $P > 0.05$, $*P < 0.05$, $**P < 0.01$, $***P < 0.001$

tumor tissues of mice treated with Conoidin A compared to the control group (Fig. 4I-J). These results suggest that inhibiting PRDX2 expression diminishes tumor cell-mediated immunosuppression.

PRDX2 promotes immune evasion by upregulating Galectin-9 expression in immune-competent mice and LUAD cells

To investigate the immunosuppression induced by PRDX2 through downstream immune checkpoints, we performed RNA sequencing analyses of the human lung adenocarcinoma cell lines sh-PRDX2 H1975 and sh-NC H1975. We focused on 50 genes encoding proteins acting as immune checkpoints [25], chemokines, and chemokine receptors, including LGALS9, CD274, PVR, IL-6, and others. Among these candidate immune molecules, LGALS9 exhibited the highest relevance (Fig. 5A). This finding was further confirmed through RT-qPCR and Western blot. The results indicated a down-regulation of Galectin-9 expression at mRNA and protein levels in the sh-PRDX2 group compared to the sh-NC group (Fig. 5B-D). Additionally, immunohistochemistry of tumor tissues from C57BL/6 mice revealed a significant decrease in Galectin-9 expression in the Conoidin A treatment group compared to the control group (Supplementary Fig. 3A).

To further ascertain the impact of Galectin-9 on the anti-tumor response of T cells, we generated three si-RNAs targeting LGALS9 to suppress the expression of LGALS9 in LUAD cell lines. The knockdown of si-LGALS9#3 proved the most effective, as confirmed by RT-qPCR experiments in H1975 and H292 cell lines (Supplementary Fig. 3B-C), and was chosen for subsequent experiments. Subsequently, we conducted in vitro co-culture of the LUAD cell line with T cells. Flow cytometry analysis indicated a significantly higher rate of tumor cell apoptosis in the si-LGALS9 group compared to the si-NC group (Fig. 5E-F). Similarly, Western blot analysis revealed an increase in the expression of cleaved-PARP and cleaved-Caspase3 proteins following the knockdown of LGALS9 (Fig. 5G-H). Immunofluorescence results

demonstrated a decrease in Galectin-9 expression and an increase in CD8⁺ T cell infiltration in the tumor tissues of mice post-treatment with Conoidin A. Furthermore, a negative correlation was found between Galectin-9 expression and the infiltration of CD8⁺ T cells (Fig. 5I-J). These findings indicate that Galectin-9 may act to inhibit the anti-tumor immune response of T cells.

HDAC3 serves as a downstream effector of PRDX2 to upregulate Galectin-9 expression

To demonstrate the regulatory role of PRDX2 in Galectin-9 expression in LUAD cells, we searched the TRRUST database for related transcription factors (TFs) and reviewed previous studies. As a result, HDAC3 was found to be the most promising candidate factor. To confirm this, we determined the protein expression of HDAC3 and phosphorylated HDAC3 in PRDX2 knockdown LUAD cells by Western blotting and detected the expression and localization of PRDX2, phosphorylated HDAC3, and Galectin-9 by immunofluorescence. Our findings, as depicted in Fig. 6A-D, revealed no significant change in total HDAC3 protein levels in the cells after PRDX2 knockdown, while the expression of phosphorylated HDAC3 protein was notably reduced. Immunofluorescence results further indicated that tumor tissues of mice in the saline-treated group exhibited high levels of PRDX2 expression and elevated levels of p-HDAC3 and Galectin-9 expression. In contrast, Conoidin A treatment lowered PRDX2 expression levels and inhibited the expression of p-HDAC3 and Galectin-9 (Fig. 6E-F). In conclusion, PRDX2 influenced Galectin-9 expression by regulating the phosphorylation of HDAC3, thereby inhibiting the anti-tumor effects of T cells and leading to tumor immune evasion. Conversely, inhibition of PRDX2 promoted the anti-tumor effects of T cells (Fig. 7).

Discussion

PRDX2 is an antioxidant enzyme in the peroxiredoxin family, which is pivotal in regulating H₂O₂ and ROS levels to safeguard cells from oxidative stress [14]. Previous

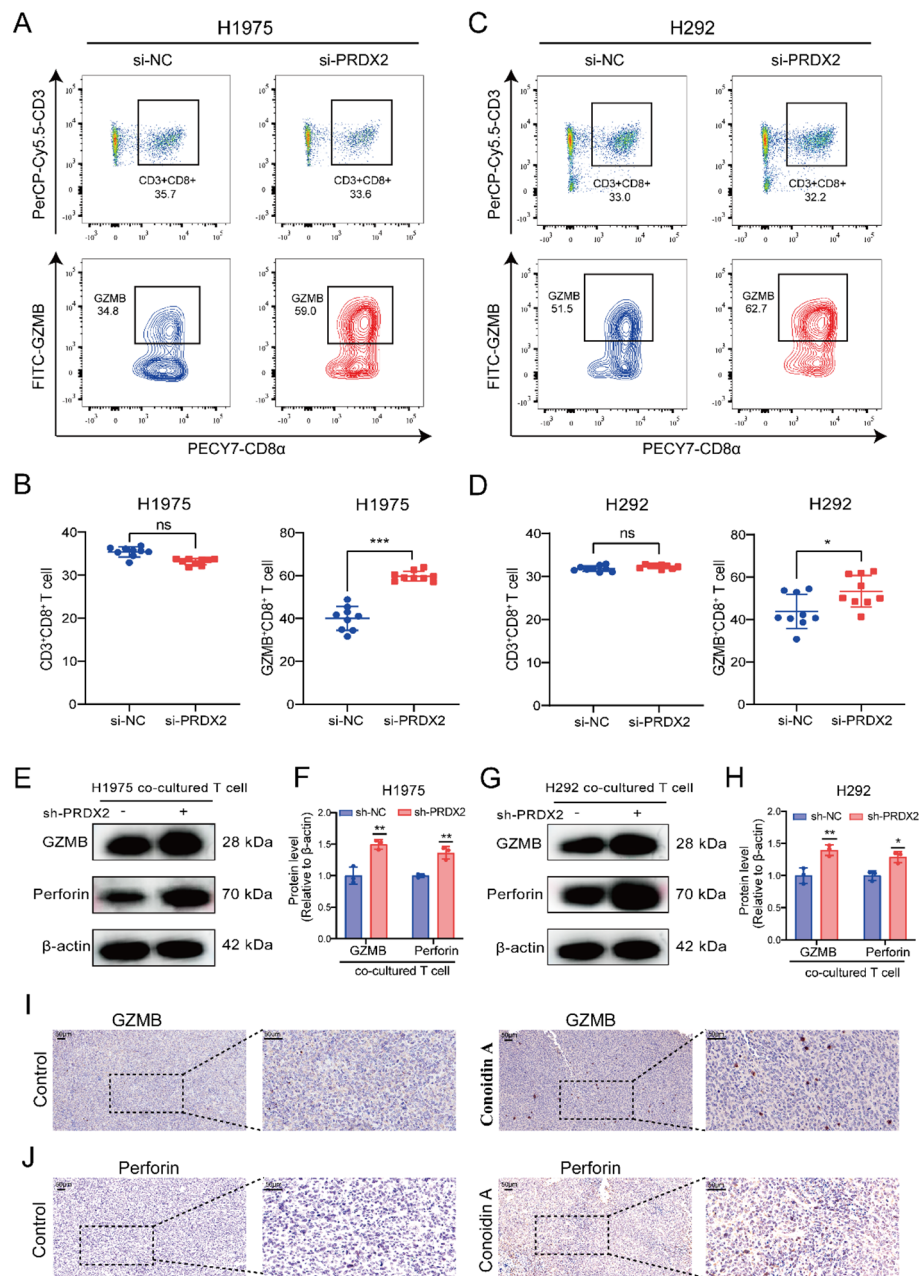


Fig. 4 Depletion of PRDX2 promotes CD8⁺CTL-mediated tumor cell killing. (A–D) Representative graphs and statistical quantification of GZMB expression in T cells after co-culture with LUAD with or without knockdown of PRDX2 detected by flow cytometry. (A) Representative images of GZMB after co-culture with H1975 cells. (B) Statistical quantitative analysis of the percentage of CD3⁺CD8⁺ T cells after co-culture with H1975 cells (left) and the percentage of GZMB⁺CD8⁺ T cells (right). (C) Representative images of GZMB after co-culture with H292 cells. (D) Statistical quantitative analysis of the percentage of CD3⁺CD8⁺ T cells (left) and the percentage of GZMB⁺CD8⁺ T cells (right) after co-culture with H292 cells. (E–H) Western blot detection of protein expression of GZMB and Perforin in T cells after co-culture with LUAD, with or without knockdown of PRDX2, along with their statistical quantitative analysis. (E) T cell GZMB and Perforin protein blots after co-culture with H1975 cells. (F) Protein grayscale quantification plots. (G) T cell GZMB and Perforin protein blots after co-culture with H292 cells. (H) Protein grayscale quantification. (I–J) IHC staining of tumor tissues from mice in Control and 10 mg/Kg Conoidin A treatment groups. (I) Graphical representation of IHC staining results of GZMB in tumor tissues. (J) Graphical representation of IHC staining results of Perforin in tumor tissues. Scale bar = 50 μ m. ns, not significant; $P > 0.05$, * $P < 0.05$, ** $P < 0.01$, *** $P < 0.001$

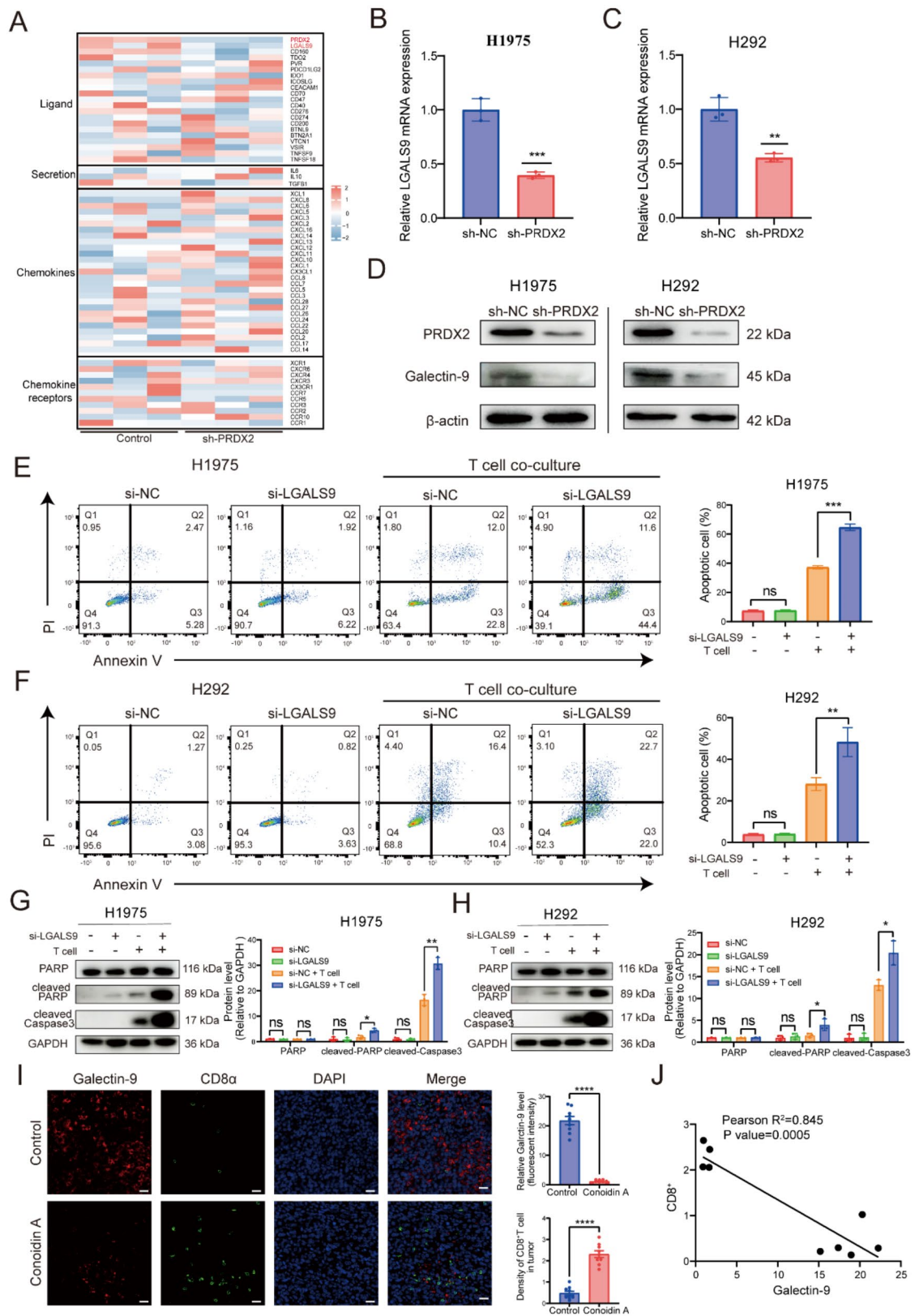


Fig. 5 (See legend on next page.)

(See figure on previous page.)

Fig. 5 Knocking down PRDX2 enhances T-cell-mediated anti-tumor immune response by suppressing LGALS9 expression. **(A)** Heatmaps of immunomodulatory molecules were visualized after RNA-Seq analysis of the H1975 cell line with stable knockdown of PRDX2. **(B)** RT-qPCR analysis of LGALS9 gene mRNA expression after PRDX2 knockdown in the H1975 cell line. **(C)** RT-qPCR analysis of LGALS9 gene mRNA expression after PRDX2 knockdown in the H292 cell line. **(D)** Western blot analysis of Galectin-9 protein expression after PRDX2 knockdown in H1975 and H292 cell lines. **(E-F)** Representative images and statistical quantification of T cell-mediated apoptosis in LUAD cells by flow cytometry analysis of T cell-mediated apoptosis determined by Annexin V-FITC and propidium iodide (PI) dual-labeling. **(E)** Apoptosis images of knockdown or non-knockdown LGALS9 H1975 cell lines (left) and their statistical quantification plots (right). **(F)** Apoptosis images of knockdown or non-knockdown LGALS9 H292 cell lines (left) and their statistical quantification plots (right). **(G-H)** Detection of apoptotic protein expression in LUAD cells co-cultured with activated T cells for 48 h by Western blot. **(G)** Protein blot of PARP, cleaved-PARP, cleaved-caspase3 in H1975 cell line with or without LGALS9 knockdown (left) and its statistical quantification analysis (right). **(H)** Protein blot of PARP, cleaved-PARP, cleaved-caspase3 in H292 cell line with or without LGALS9 knockdown (left) and its statistical quantification analysis (right). **(I)** Immunofluorescence staining and quantification of relative expression of Galectin-9 protein and CD8⁺ T cells in tumor tissues of mice in the Control group and 10 mg/Kg Conoidin A treatment group. Galectin-9 protein (Galectin-9, red), CD8⁺ T cells (CD8 α , green), and nuclear staining (DAPI, blue). Three mice per group were selected for IF staining and three fields of view per mouse were selected for analysis, with each dot representing one field of view. Scale bar = 20 μ m. **(J)** Analysis of the correlation between Galectin-9 and CD8 expression. ns, not significant; $P > 0.05$, $*P < 0.05$, $**P < 0.01$, $***P < 0.001$, $****P < 0.0001$

research has demonstrated that PRDX2, besides its antioxidant capacity, is overexpressed in various cancers and is involved in several processes of cancer progression [26], including regulating cell proliferation, apoptosis, drug resistance, and signaling [27–29]. Studies have indicated that PRDX2 promotes the proliferation of hepatocellular carcinoma cells by activating the Ras/Raf/MEK/ERK/FoxM1/cyclin D1 cascade [30]. Additionally, PRDX2 binds to RPL4, impedes RPL4-MDM2 binding, and leads to the degradation of p53, ultimately promoting the proliferation of colorectal cancer cells [29]. Moreover, the overexpression of PRDX2 serves as a poor prognostic marker for cisplatin-resistant gastric cancer [31]. Previous reports have also highlighted the association between PRDX2 and immune infiltration of tumors, with PRDX2 consistently elevated in colon adenocarcinoma and negatively correlated with immune infiltration in COAD [32]. Our research showed a significant increase in PRDX2 expression in LUAD. This upregulation of PRDX2 was strongly linked to the prognosis of LUAD patients and was associated with a decrease in CD8⁺ T cell infiltration. Our in vivo studies in immunodeficient BALB/c nude mice showed no significant difference in tumor growth inhibition between control and Conoidin A treatments. In contrast, in immune-competent C57BL/6 mice, treatment with Conoidin A inhibited tumor growth and enhanced the infiltration and killing function of CD3⁺CD8⁺ T cells. Furthermore, in vitro studies have demonstrated that PRDX2 deficiency in tumor cells significantly augments T cell-mediated cytotoxicity, suggesting its critical role in immune evasion within LUAD cells.

Inhibitors targeting the PD-1 and CTLA-4 immune checkpoints have emerged as a potent strategy for treating a wide range of cancers by enhancing the cytotoxic activity of host T cells by blocking inhibitory

signals from tumor cells. However, only a small number of patients have shown a response [33]. Galectin-9 is highly expressed in various human malignancies, including pancreatic ductal adenocarcinoma [34], breast cancer [35], hepatocellular carcinoma [36], and colorectal carcinoma [37]. Galectin-9 serves as a ligand for Tim-3, and the Tim-3/Gal-9 pathway leads to cell death, particularly depletion of effector T cells or apoptosis, and the subsequent establishment of immune tolerance [38, 39]. Galectin-9 can also impede innate immunity by downregulating the functions of natural killer cells (NK cells) [40]. Not coincidentally, our study discovered that inhibition of Galectin-9 expression in LUAD tumor cells resulted in a significant increase in tumor cell apoptosis after co-culture with T cells in vitro. In vivo studies revealed that Galectin-9 expression decreased in tumor tissues after treatment with Conoidin A, and Galectin-9 expression was negatively correlated with CD8⁺ T cells. Therefore, our study reveals a novel immunosuppressive role of PRDX2 in LUAD.

Histone deacetylase 3 (HDAC3) is a member of the class I HDAC family with four splice variants, HD3 α , β , γ , and δ [41]. Previous research has indicated that HDAC3 can regulate the expression of Galectin-9, and inhibiting HDAC3 activity leads to reduced Galectin-9 expression [42]. Furthermore, phosphorylation at the HDAC3 Ser 424 site is necessary for HDAC3 enzymatic activity [43]. This study observed that blockade of PRDX2 on LUAD cells inhibited phosphorylated HDAC3, which decreased Galectin-9 expression, ultimately reduced tumor immune evasion, and promoted infiltration and clearance of activated T cells. The discovery of the PRDX2/HDAC3/Galectin-9 regulatory axis deepens our understanding of the mechanism of immune evasion in LUAD cells.

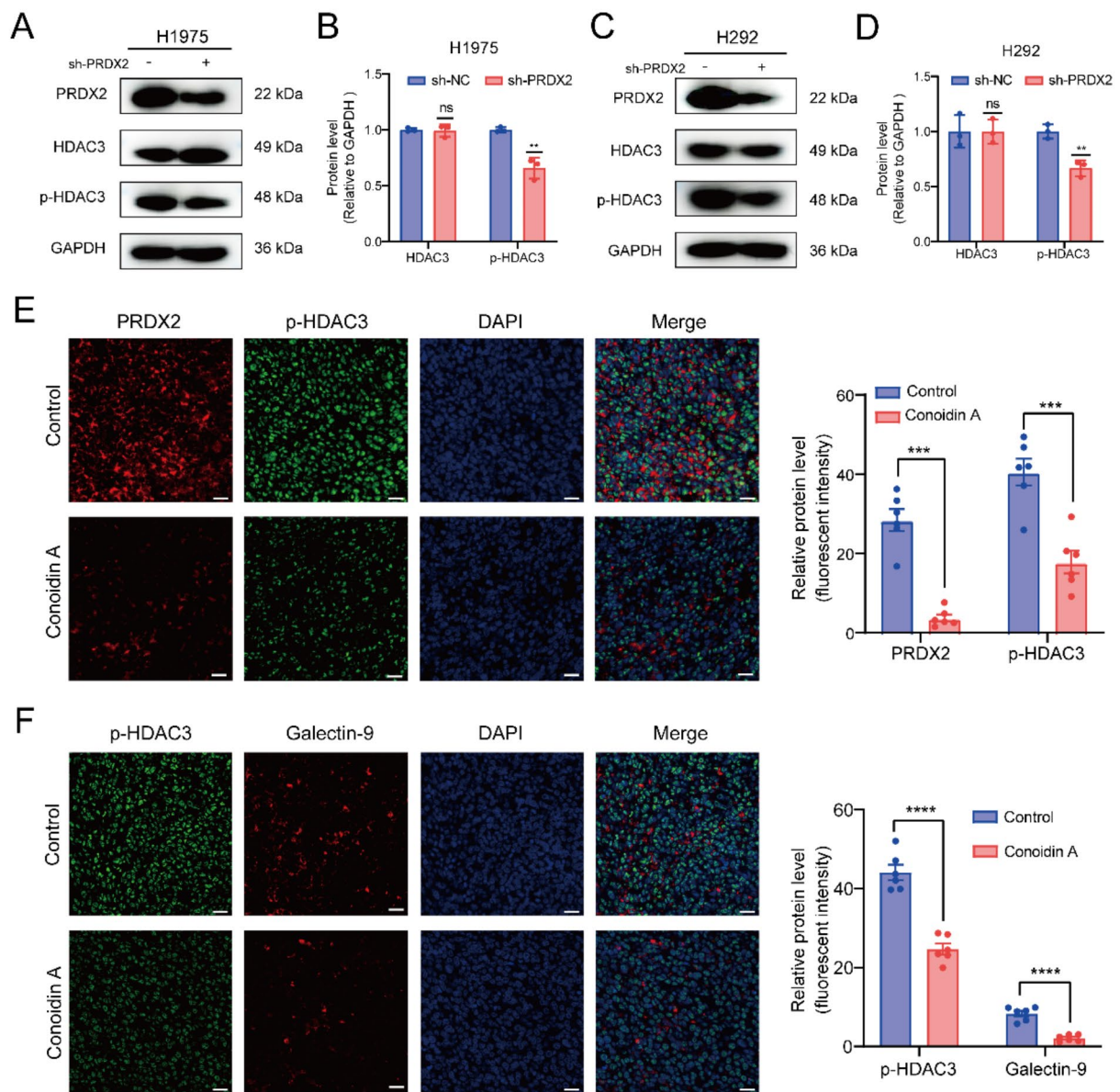


Fig. 6 PRDX2 regulates the expression of LGALS9 through HDAC3. (A-D) Western blot detects HDAC3 protein expression in knockdown and non-knockdown PRDX2 LUAD cells. (A) Protein blot of HDAC3 and phospho-HDAC3 in the H1975 cell line. (B) Protein grayscale quantification plots. (C) Protein blot of HDAC3 and phospho-HDAC3 in the H292 cell line. (D) Protein grayscale quantification plots. (E) Immunofluorescence staining and quantification of relative expression of PRDX2 and p-HDAC3 proteins in tumor tissues of mice in Control and 10 mg/Kg Conoidin A treatment groups. PRDX2 protein (PRDX2, red), p-HDAC3 protein (p-HDAC3, green), and nuclear staining (DAPI, blue). Three mice per group were selected for IF staining and two fields of view per mouse were selected for analysis, with each dot representing one field of view. Scale bar = 20 μ m. (F) Immunofluorescence staining and quantification of relative expression of Galectin-9 and p-HDAC3 proteins in tumor tissues of mice in the Control group and 10 mg/Kg Conoidin A treatment group. Galectin-9 protein (Galectin-9, red), p-HDAC3 protein (p-HDAC3, green), and nuclear staining (DAPI, blue). Three mice per group were selected for IF staining and two fields of view per mouse were selected for analysis, with each dot representing one field of view. Scale bar = 20 μ m. ns, not significant; $P > 0.05$, $*P < 0.05$, $**P < 0.01$, $***P < 0.001$, $****P < 0.0001$

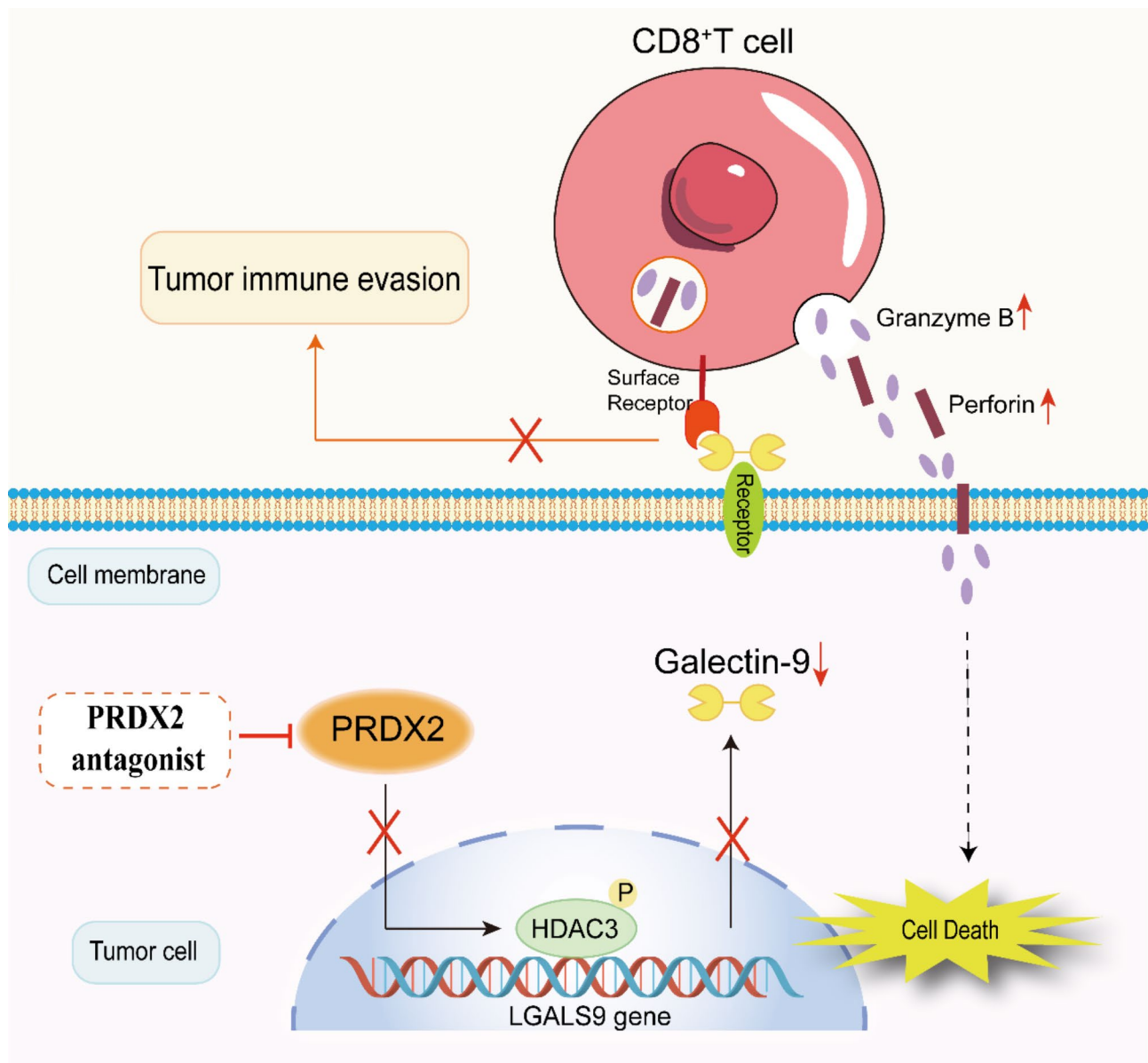


Fig. 7 Model of PRDX2-mediated immunosuppressive effect in LUAD. PRDX2 is highly expressed in LUAD and upregulates Galectin-9 expression through HDAC3. Galectin-9 binds to inhibitory receptors on the surface of T cells, thereby inhibiting T cell function and ultimately causing immune evasion

Conclusions

This study suggests that the PRDX2/HDAC3 axis ultimately promotes immune evasion of LUAD cells by increasing Galectin-9 expression. The finding that inhibition of PRDX2 enhances CD8⁺ T-cell infiltration and cytotoxicity expands our understanding of the role of PRDX2 in LUAD antitumor immunity. It provides a promising therapeutic approach for LUAD immunotherapy.

Supplementary Information

The online version contains supplementary material available at <https://doi.org/10.1186/s12967-024-05888-z>.

Supplementary Material 1

Acknowledgements

This study was sponsored by the Research Funds of Joint Research Center for Occupational Medicine and Health of IHM(OMH-2023-09); and Medical Special Cultivation Project of Anhui University of Science and Technology (YZ2023H2A001, YZ2023H1A006). The funders had no role in the study design, data collection, analysis, and decision to publish or preparation of the manuscript.

Author contributions

WJ, and HD: conception and design, and study supervision. DY, CA, ZJ, GJ, LY, LX and CM: development of methodology, analysis and interpretation of data, and writing of the manuscript. DY: review of the manuscript.

Data availability

The data supporting the conclusions of this article have been provided in this article and its supplementary Files. In addition, all data from this study can be obtained from the corresponding author upon reasonable request.

Declarations

Ethics approval and consent to participate

This study was approved by the medical ethics committee of Anhui University of Science and Technology (NO. HX-002).

Consent for publication

The content of the article, authorship and ranking of all authors have been carefully reviewed and agreed to publish.

Competing interests

The authors declare that they have no known competing financial interests or personal relationships that could have appeared to influence the work reported in this paper.

Received: 9 May 2024 / Accepted: 14 November 2024

Published online: 17 January 2025

References

1. Siegel RL, Miller KD, Wagle NS, Jemal A. Cancer statistics, 2023. *CA Cancer J Clin.* 2023;73(1):17–48.
2. Herbst RS, Morgensztern D, Boshoff C. The biology and management of non-small cell lung cancer. *Nature.* 2018;553(7689):446–54.
3. Planchard D, Popat S, Kerr K, Novello S, Smit EF, Faivre-Finn C, et al. Metastatic non-small cell lung cancer: ESMO Clinical Practice guidelines for diagnosis, treatment and follow-up. *Ann Oncol.* 2018;29(Suppl 4):iv192–237.
4. Garon EB, Rizvi NA, Hui R, Leighl N, Balmanoukian AS, Eder JP, et al. Pembrolizumab for the treatment of non-small-cell lung cancer. *N Engl J Med.* 2015;372(21):2018–28.
5. Reck M, Remon J, Hellmann MD. First-line immunotherapy for non-small-cell Lung Cancer. *J Clin Oncol.* 2022;40(6):586–97.
6. Wang DR, Wu XL, Sun YL. Therapeutic targets and biomarkers of tumor immunotherapy: response versus non-response. *Signal Transduct Target Ther.* 2022;7(1):331.
7. Ansell SM, Lesokhin AM, Borrello I, Halwani A, Scott EC, Gutierrez M, et al. PD-1 blockade with nivolumab in relapsed or refractory Hodgkin's lymphoma. *N Engl J Med.* 2015;372(4):311–9.
8. Hodi FS, O'Day SJ, McDermott DF, Weber RW, Sosman JA, Haanen JB, et al. Improved survival with ipilimumab in patients with metastatic melanoma. *N Engl J Med.* 2010;363(8):711–23.
9. Robert C, Thomas L, Bondarenko I, O'Day S, Weber J, Garbe C, et al. Ipilimumab plus dacarbazine for previously untreated metastatic melanoma. *N Engl J Med.* 2011;364(26):2517–26.
10. Brahmer JR, Tykodi SS, Chow LQ, Hwu WJ, Topalian SL, Hwu P, et al. Safety and activity of anti-PD-L1 antibody in patients with advanced cancer. *N Engl J Med.* 2012;366(26):2455–65.
11. Nelson KJ, Knutson ST, Soito L, Klomsiri C, Poole LB, Fetrow JS. Analysis of the peroxiredoxin family: using active-site structure and sequence information for global classification and residue analysis. *Proteins.* 2011;79(3):947–64.
12. Hall A, Karplus PA, Poole LB. Typical 2-Cys peroxiredoxins—structures, mechanisms and functions. *FEBS J.* 2009;276(9):2469–77.
13. Wood ZA, Schroder E, Robin Harris J, Poole LB. Structure, mechanism and regulation of peroxiredoxins. *Trends Biochem Sci.* 2003;28(1):32–40.
14. De Franceschi L, Bertoldi M, De Falco L, Santos Franco S, Ronzoni L, Turrini F, et al. Oxidative stress modulates heme synthesis and induces peroxiredoxin-2 as a novel cytoprotective response in beta-thalassemic erythropoiesis. *Haematologica.* 2011;96(11):1595–604.
15. Zhang S, He J, Tang M, Sun H. Prdx2 Upregulation promotes the growth and survival of gastric Cancer cells. *Pathol Oncol Res.* 2020;26(3):1869–77.
16. Zheng X, Wei J, Li W, Li X, Wang W, Guo J, et al. PRDX2 removal inhibits the cell cycle and autophagy in colorectal cancer cells. *Aging.* 2020;12(16):16390–409.
17. Chen Y, Yang S, Zhou H, Su D. PRDX2 promotes the proliferation and metastasis of Non-small Cell Lung Cancer in Vitro and in vivo. *Biomed Res Int.* 2020;2020:8359860.
18. Yang RY, Rabinovich GA, Liu FT. Galectins: structure, function and therapeutic potential. *Expert Rev Mol Med.* 2008;10:e17.
19. Okoye I, Xu L, Motamedi M, Parashar P, Walker JW, Elahi S. Galectin-9 expression defines exhausted T cells and impaired cytotoxic NK cells in patients with virus-associated solid tumors. *J Immunother Cancer.* 2020;8(2).
20. Zhu C, Anderson AC, Schubart A, Xiong H, Imitola J, Khoury SJ, et al. The Tim-3 ligand galectin-9 negatively regulates T helper type 1 immunity. *Nat Immunol.* 2005;6(12):1245–52.
21. Zheng S, Song J, Linghu D, Yang R, Liu B, Xue Z, et al. Galectin-9 blockade synergizes with ATM inhibition to induce potent anti-tumor immunity. *Int J Biol Sci.* 2023;19(3):981–93.
22. Moar P, Tandon R. Galectin-9 as a biomarker of disease severity. *Cell Immunol.* 2021;361:104287.
23. Morris G, Walker AJ, Berk M, Maes M, Puri BK. Cell death pathways: a Novel Therapeutic Approach for neuroscientists. *Mol Neurobiol.* 2018;55(7):5767–86.
24. Agarwal A, Mahfouz RZ, Sharma RK, Sarkar O, Mangrola D, Mathur PP. Potential biological role of poly (ADP-ribose) polymerase (PARP) in male gametes. *Reprod Biol Endocrinol.* 2009;7:143.
25. Fang J, Chen F, Liu D, Gu F, Chen Z, Wang Y. Prognostic value of immune checkpoint molecules in breast cancer. *Biosci Rep.* 2020;40(7).
26. Park MH, Jo M, Kim YR, Lee CK, Hong JT. Roles of peroxiredoxins in cancer, neurodegenerative diseases and inflammatory diseases. *Pharmacol Ther.* 2016;163:1–23.
27. Chen X, Zhao Y, Luo W, Chen S, Lin F, Zhang X, et al. Celastrol induces ROS-mediated apoptosis via directly targeting peroxiredoxin-2 in gastric cancer cells. *Theranostics.* 2020;10(22):10290–308.
28. Feng AL, Han X, Meng X, Chen Z, Li Q, Shu W, et al. PRDX2 plays an oncogenic role in esophageal squamous cell carcinoma via Wnt/beta-catenin and AKT pathways. *Clin Transl Oncol.* 2020;22(10):1838–48.
29. Wang W, Wei J, Zhang H, Zheng X, Zhou H, Luo Y, et al. PRDX2 promotes the proliferation of colorectal cancer cells by increasing the ubiquitinated degradation of p53. *Cell Death Dis.* 2021;12(6):605.
30. Park YH, Kim SU, Kwon TH, Kim JM, Song IS, Shin HJ, et al. Peroxiredoxin II promotes hepatic tumorigenesis through cooperation with Ras/Forkhead box M1 signaling pathway. *Oncogene.* 2016;35(27):3503–13.
31. Wang S, Chen Z, Zhu S, Lu H, Peng D, Soutto M, et al. PRDX2 protects against oxidative stress induced by H. Pylori and promotes resistance to cisplatin in gastric cancer. *Redox Biol.* 2020;28:101319.
32. Zhang X, Gao F, Li N, Zhang J, Dai L, Yang H. Peroxiredoxins and Immune infiltrations in Colon adenocarcinoma: their negative correlations and clinical significances, an in Silico Analysis. *J Cancer.* 2020;11(11):3124–43.
33. Thanarajasingam G, Thanarajasingam U, Ansell SM. Immune checkpoint blockade in lymphoid malignancies. *FEBS J.* 2016;283(12):2233–44.
34. Seifert AM, Reiche C, Heiduk M, Tannert A, Meinecke AC, Baier S, et al. Detection of pancreatic ductal adenocarcinoma with galectin-9 serum levels. *Oncogene.* 2020;39(15):3102–13.
35. Yasinska IM, Sakhnevych SS, Pavlova L, Teo Hansen Selno A, Teuscher Abeleira AM, Benlaouer O, et al. The Tim-3-Galectin-9 Pathway and its Regulatory mechanisms in human breast Cancer. *Front Immunol.* 2019;10:1594.
36. Fujita K, Iwama H, Sakamoto T, Okura R, Kobayashi K, Takano J, et al. Galectin-9 suppresses the growth of hepatocellular carcinoma via apoptosis in vitro and in vivo. *Int J Oncol.* 2015;46(6):2419–30.
37. Sasidharan Nair V, Toor SM, Taha RZ, Shaath H, Elkord E. DNA methylation and repressive histones in the promoters of PD-1, CTLA-4, TIM-3, LAG-3, TIGIT, PD-L1, and galectin-9 genes in human colorectal cancer. *Clin Epigenetics.* 2018;10(1):104.
38. Sakuishi K, Jayaraman P, Behar SM, Anderson AC, Kuchroo VK. Emerging Tim-3 functions in antimicrobial and tumor immunity. *Trends Immunol.* 2011;32(8):345–9.
39. Schlichtner S, Yasinska IM, Lall GS, Berger SM, Ruggiero S, Cholewa D et al. T lymphocytes induce human cancer cells derived from solid malignant tumors to secrete galectin-9 which facilitates immunosuppression in cooperation with other immune checkpoint proteins. *J Immunother Cancer.* 2023;11(1).
40. Golden-Mason L, McMahan RH, Strong M, Reisdorph R, Mahaffey S, Palmer BE, et al. Galectin-9 functionally impairs natural killer cells in humans and mice. *J Virol.* 2013;87(9):4835–45.

41. Gray SG, Ekstrom TJ. The human histone deacetylase family. *Exp Cell Res.* 2001;262(2):75–83.
42. Alam S, Li H, Margariti A, Martin D, Zampetaki A, Habi O, et al. Galectin-9 protein expression in endothelial cells is positively regulated by histone deacetylase 3. *J Biol Chem.* 2011;286(51):44211–7.
43. Zhang X, Ozawa Y, Lee H, Wen YD, Tan TH, Wadzinski BE, et al. Histone deacetylase 3 (HDAC3) activity is regulated by interaction with protein serine/threonine phosphatase 4. *Genes Dev.* 2005;19(7):827–39.

Publisher's note

Springer Nature remains neutral with regard to jurisdictional claims in published maps and institutional affiliations.